Pharm Res (2010) 27:2657–2669
DOI 10.1007/s11095-010-0265-9

RESEARCH PAPER

Poly(ε-caprolactone)-*Block*-poly(ethyl Ethylene Phosphate) Micelles for Brain-Targeting Drug Delivery: *In Vitro* and *In Vivo* Valuation

Pengcheng Zhang • Luojuan Hu • Yucai Wang • Jun Wang • Linyin Feng • Yaping Li

Received: 13 June 2010 / Accepted: 30 August 2010 / Published online: 18 September 2010

ABSTRACT

Purpose The purpose of this work was to investigate the potential of poly(ε-caprolactone)-*block*-poly(ethyl ethylene phosphate) (PCL-PEEP) micelles for brain-targeting drug delivery.

Method The coumarin-6-loaded PCL-PEEP micelles (CMs) were prepared and characterized. The cellular uptake of CMs was evaluated on *in vitro* model of brain-blood barrier (BBB), and the brain biodistribution of CMs in ICR mice was investigated.

Results PCL-PEEP could self-assemble into 20 nm micelles in water with the critical micelle concentration (CMC) 0.51 μg/ml and high coumarin-6 encapsulation efficiency (92.5 ± 0.7%), and the micelles were stable in 10% FBS with less than 25% leakage of incorporated coumarin-6 during 24 h incubation at 37°C. The cellular uptake of CMs by BBB model was significantly higher and more efficient than coumarin-6 solution (CS) at 50 ng/ml. Compared with CS, 2.6-fold of coumarin-6 was found in the brains of CM-treated mice, and C_{max} of CMs was 4.74% of injected dose/g brain. The qualitative investigation on the brain distribution of CMs indicated that CMs were prone to accumulate in hippocampus and striatum.

Conclusion These results suggest that PCL-PEEP micelles could be a promising brain-targeting drug delivery system with low toxicity.

KEY WORDS biodistribution · blood-brain barrier (BBB) · micelle · polyphosphoester

INTRODUCTION

The blood-brain barrier (BBB) is the most formidable obstacle in the treatment of brain disorder because BBB excludes more than 98% of small-molecule drugs and almost 100% of large-molecule drugs (1). So far, the strategies to deliver drugs with poor BBB permeability mainly include invasive and noninvasive approaches. Invasive approaches, such as direct injection or infusion, are effective, but this method is associated with risk of infection, high neurosurgical cost and a limited delivery area (2). Noninvasive approaches, such as developing BBB-permeable prodrugs or ligand-drug conjugation, show some interesting results, but also demonstrate drawbacks including loss of therapeutic effect. Nanocarrier-based receptor-mediated transcytosis (RMT) is the most extensively employed strategy in noninvasive central nervous system (CNS)-targeting drug delivery and increases the brain accumulation of medicaments (3). However, RMT requires the coupling of carriers with ligands which are usually expensive purified proteins, and the percent of injected dose (ID) accumulated in brain is also relatively low (less than 1% ID/g brain) (4–9). Aside from the

Pengcheng Zhang and Luojuan Hu contributed equally to this work.

P. Zhang • Y. Li (✉)
Center of Pharmaceutics, Shanghai Institute of Materia Medica
Chinese Academy of Sciences
501 Haike Road
Shanghai 201203, China
e-mail: ypli@mail.shcnc.ac.cn

L. Hu • L. Feng (✉)
State Key Laboratory of Drug Research
Shanghai Institute of Materia Medica
Chinese Academy of Sciences
555 Zuchongzhi Road
Shanghai 201203, China
e-mail: lyfeng@mail.shcnc.ac.cn

Y. Wang • J. Wang
University of Sciences and Technology of China
Hefei 230026, China

RMT strategy, the brain accumulation of drugs could also be increased by decreasing particle size (10, 11), which is more feasible at least from the clinical point of view.

Polymeric micelles show great potential in biological and pharmaceutical applications (12). Thus, micelles composed of poly(ethylene glycol)-poly(glutamic acid), poly(ethylene glycol)-cholesterol or poly(ethylene glycol)-poly(lactide) have been investigated as brain-targeted carriers (4, 13, 14). Although poly(ethylene glycol) (PEG) can be eliminated by kidney and has been proven to be safe at relatively high doses (15), it is undegradable in physiological condition. Furthermore, its brain elimination rate and the effect of PEG brain accumulation have not been investigated because PEG itself could not cross BBB after intravenous injection. Therefore, it is still a big challenge to develop efficient CNS-targeting carriers with low toxicity (2).

Polyphosphoester (PPE) is a class of biodegradable polymers with repeated phosphoester linkage in the backbone which degrades under physiological condition via hydrolysis or enzymatic cleavage of the phosphoester bonds (16), and PPE showed good biocompatibility to neuron (17). In addition, PPE can be easily modified by varying the side chains, which facilitates its further application in drug, gene delivery and tissue engineering (18). Furthermore, the polymer can be further functionalized to increase the cellular uptake of drug in specific cells (19). Poly(ethyl ethylene phosphate) (PEEP) is a hydrophilic derivative of PPE, which can copolymerize with poly(ε-caprolactone) (PCL) to obtain an amphiphilic block copolymer, and the particle size of micelles composed of PCL-PEEP can be tuned by varying the length of PCL (20). As a result, we presumed that PCL-PEEP could have good potential for drug delivery, especially targeted to CNS.

In order to prove whether PCL-PEEP could especially target to CNS, in the present work, PCL-PEEP micelles incorporating coumarin-6 were prepared and characterized. Coumarin-6 was chosen because of its hydrophobicity, high detection sensitivity, pH-independent release and wide application for the evaluation of brain-targeting drug delivery systems (4, 8, 21). The cellular uptake and toxicity of micelles were investigated on the *in vitro* model of BBB. The brain distribution of micelles on ICR mice was evaluated qualitatively with fluorescence microscope and quantitatively with fluorometer.

MATERIALS AND METHODS

Materials

Coumarin-6 was purchased from Acros Organics (Belgium), and Tween-80 was obtained from Sigma-Aldrich (USA). EMB-2 Endothelial Growth Medium with supplements and growth factors was obtained from Lonza (Switzerland). Primary anti-von Willebrand factor antibody was obtained from Abcam (Britain), and the other antibodies used in immunocytochemistry were from Invitrogen (USA). Tetrahydrofuran (THF) was refluxed over potassium and sodium alloy under N_2 atmosphere and distilled out just before use. Stannous octoate ($Sn(Oct)_2$) was purified according to the method described in literature (22). All other reagents were of analytical grade and used as received.

Ethyl ethylene phosphate (EEP) and macroinitiator PCL bearing one hydroxyl group per polymer chain were synthesized and purified as previously reported (22). The obtained PCL-OH was then characterized by a 300 MHz ^{1}H NMR spectrometer (Varian, USA), and the average degree of polymerization of the macroinitiator was 31 according to the integration ratio of peaks at 4.07 and 3.67 ppm. The obtained PCL-OH was therefore termed PCL_{31}-OH.

Animals

ICR mice (18~22 g, ♂) and Sprague-Dawley (SD) rats (4-week at age, ♂) were obtained from Shanghai Experiment Animal Center, Chinese Academy of Sciences, and maintained at 25±2°C on a 12 h light-dark cycle with free access to food and water. All animal procedures were performed following the protocol approved by the Institutional Animal Care and Use Committee at Shanghai Institute of Materia Medica, Chinese Academy of Sciences.

Synthesis and Characterization of PCL-PEEP

PCL-PEEP was synthesized by initiating the ring-opening polymerization of EEP with PCL_{31}-OH using $Sn(Oct)_2$ as the catalyst (20). Briefly, $Sn(Oct)_2$ (1.0 g, 2.5 mmol) was added to a solution of EEP (18.5 g, 121.7 mmol) and PCL_{31}-OH (9.1 g, 2.5 mmol) in THF at 35°C. After 5 h, the mixture was concentrated and precipitated in cold ethyl ester twice to obtain PCL-PEEP. The PCL-PEEP was dissolved in deuterated chloroform and confirmed by a 300 MHz ^{1}H NMR spectrometer (Varian, USA). The degree of polymerization and ^{1}H NMR-based Mn were calculated according to the literature (20).

The number and average molecular weight (Mn and Mw) and molecular weight distribution (polydispersity index, PDI=Mw/Mn) of PCL-PEEP were determined by gel permeation chromatography (GPC) using a Waters GPC system equipped with a Waters 2414 refractive index detector and four Waters styragel high resolution columns (HR4, HR2, HR1, HR0.5). Chloroform was used as mobile phase with a flow rate of 1 ml/min at 40°C. The samples were analyzed and calibrated by monodispersed polysty-

rene standards with a molecular weight range of 1,130–55,100 Da.

The polymer micelles were prepared by dialysis method. Typically, 50 mg PCL-PEEP was dissolved in 500 μl THF and stirred for 10 min to obtain a clear solution. Then, 2.5 ml Milli-Q water (Milli-Q Synthesis, 18.2 MΩ) was added dropwise to the resulting solution under gentle stirring. After standing 0.5 h at room temperature, THF was removed by dialysis against 2 L Milli-Q water for 12 h using dialysis bag (MWCO = 6–8 kDa, Spectrum Laboratories Inc.). The critical micelle concentration (CMC) of PCL-PEEP was estimated using a fluorescent spectroscopic method based on the preferential partition of the pyrene probe in the hydrophobic core against an aqueous environment (20). In brief, to ampules containing pyrene, a predetermined volume of PCL-PEEP solution and ultrapurified water were consecutively added to get solutions of different micelle concentrations ranging from 1.0×10^{-5} to 0.5 g/L. The concentration of pyrene was fixed at 6.0×10^{-7} mol/L. Fluorescence spectra were recorded on a Shimadzu RF-5301PC spectrofluorophotometer at 373 nm excitation wavelength and 5 nm slit width.

Preparation and Characterization of Coumarin-6-Loaded Polymer Micelles (CMs)

Coumarin-6-loaded polymer micelles were prepared by dialysis method as described above, except 0.25 mg coumarin-6 was added to 500 μl THF solution containing 50 mg PCL-PEEP. Blank polymer micelles (BMs) were prepared for the toxicity evaluation with the same method without coumarin-6. The micelles were sterilized by 0.22 μm filter (Millipore). The particle size distribution and ζ potential of CMs were measured by Nicomp 380/ZLS zeta potential analyzer (Particle Sizing System, USA), and the morphology of CMs was characterized with atomic force microscope (AFM, Veeco Nanoscope IIIa MultiMode system, Veeco Instrument, CA). The loading amount of coumarin-6 was determined by NOVOstar microplate reader (BMG LABTECH, Germany) (Ex/Em = 450/510 nm) after dissolving lyophilized micelles with acetonitrile. The encapsulation efficiency (EE) and drug loading capacity (DLC) of CMs were defined by the following two equations.

$$\mathrm{EE}(\%) = \frac{\text{amount of coumarin-6 in CMs}}{\text{amount of coumarin-6 used for CM preparation}} \times 100\%$$

$$\mathrm{DLC}(\%) = \frac{\text{amount of coumarin-6 in CMs}}{\text{amount of CMs}} \times 100\%$$

In Vitro Release of Coumarin-6 from CMs

To evaluate the stability of CMs during *in vitro* and *in vivo* experiments, the profiles of coumarin-6 releasing from CMs were plotted in Hanks Balanced Salt Solution (HBSS, pH 7.4) and Dulbecco's Modified Eagle Medium (DMEM, Invitrogen) containing 10% FBS (Biochrom, Germany) at 37°C. CMs were incubated at 100 μg/ml coumarin-6 with a shaking at 100 rpm under a predetermined sink condition. At predetermined time points, samples were collected and centrifugated at 1×10^5 g for 1 h, and the supernatants were diluted with acetonitrile and analyzed by a spectrofluorophotometer.

Establishment and Characterization of an *In Vitro* Model of BBB

Primary rat brain microvessel endothelial cells (BMECs) were obtained from SD rat brain microvessels to establish the *in vitro* model of BBB. First, rat brain microvessels were isolated by a two-step enzymatic digest method and a sequential 50% Percoll (Pharmacia, USA) gradient centrifugation as described previously (23). The microvessels were planted on 24-well plates, coverslips or 1.12 cm^2 Transewell inserts (0.4 μm pore size) (Corning, USA), all of which were previously coated with rat tail tendon collagen Type I (Shengyou, China). After 4 h attachment, microvessels were washed three times with pre-warmed D-Hank's for further purification. EMB-2 medium (supplemented with hydrocortisone, hEGF, FBS, VEGF, hFGF-B, R3-IGF-1, ascorbic acid and gentamicin/amphotericin-B) was used thereafter to promote the cell proliferation and induce barrier properties, and 3 μg/ml puromycin was added to the medium at the first three days to specifically kill the contaminating cells with low P-glycoprotein expression.

To prove the successful establishment of the *in vitro* model of BBB, immunocytochemical method was applied to detect the expression of specific BBB markers, including von Willebrand factor (marker of endothelia cells), occludin (tight junction protein), and F-actin (cytoskeletal component), as previously described with minor modification (24). Briefly, after eight days incubation, BMECs on coverslips were fixed for 5 min with iced acetone-methanol solution (1:1, *v/v*), rinsed with PBS three times, permeated with 0.2% Trition X-100 in PBS for 5 min, and finally blocked for 2 h in blocking buffer (5% normal goat serum, 1% BSA, 0.1% Triton X-100 and 0.1% sodium azide in PBS). Subsequently, primary antibodies (rabbit anti-human von Willebrand factor (1/40), rabbit anti-occluding (1/25)) diluted in block solution were incubated with samples overnight at 4°C. Nonbinding antibodies were washed off with PBS before the addition of secondary antibodies (Alexa Flour 488 goat anti-rabbit IgG antibody (1/200) and Alexa Flour 610 goat anti-

rabbit IgG antibody (1/200)). For F-actin staining, Alexa Fluor 532-phalloidin (0.4 μM) was incubated with fixed cells for 15 min at room temperature. The images were acquired with a fluorescence microscope (IX51, Olympus, Japan).

The barrier property of the BBB model was evaluated with Millicell-ERS Electrical Resistance System (MERS00001, Millipore, USA). After the BMECs on 1.12 cm^2 Transewell inserts grew to confluence, the transendothelial electrical resistance (TEER) of the BMEC monolayers was monitored every other day. Final resistances (Ωcm^2) were calculated after subtracting the resistance of an empty insert without cells.

Cellular Uptake of CMs by BMECs

The time-, temperature- and concentration-dependent internalization of CMs by BMECs was investigated. BMECs were pretreated with HBSS for 30 min and incubated with HBSS-diluted CMs or coumarin-6 solution (CS, coumarin: Tween 80 = 1:250, *w/w*) containing 50 ng/ml coumarin-6 for 0.5, 1, 2 and 4 h at 4°C and 37°C, respectively. In a separate experiment, HBSS-diluted CMs or CS containing 5, 50, 200 or 500 ng/ml coumarin-6 was incubated with the cells for 2 h at 37°C. After discarding the incubation medium, the cells were washed twice with ice-cold PBS (pH 7.4) and lysed with RIPA lysis buffer for 30 min. Coumarin-6 was solubilized with equal volume of acetonitrile and determined with NOVOstar microplate reader as described above. The standard curve was constructed by adding different amounts of coumarin-6 to the cells followed with lysis and solubilization procedure as described above. The concentration of coumarin-6 was normalized with the amount of cellular protein which was determined by coomassie brilliant blue method.

Toxicity of BMs on BBB Model

The cytotoxicity of BMs to primary BMECs was evaluated by MTT assay. BMECs were seeded in 24-well plates coated with rat tail tendon collagen Type I and incubated for 5 days. Then, different amounts of BMs were added to achieve the final concentration of 0, 0.02, 0.05, 0.1, 0.2, 0.5, 1 or 2 mg/ml. After 24 h incubation, the medium was refreshed with medium containing 0.5 mg/ml MTT followed with 4 h incubation. Thereafter, the medium was carefully removed, and 400 μl DMSO was added to dissolve the formazan. Absorbance was measured at 570 nm using NOVOstar microplate reader. Cell viability was expressed as percentage of absorbance in comparison with that of non-treated cells.

To determine if the micelles affect the integrity of BBB model, the TEER of the model was monitored. The model with TEER above 300 Ωcm^2 was incubated with 2 mg/ml BMs for 24 h. Then, the medium was replaced with fresh endothelial growth media, and the TEER of BBB model was recorded again after 48 h.

Brain Distribution of CMs

For quantitative study, 56 ICR mice were randomly divided into two groups, dosed with CMs or CS at 0.4 mg/kg via caudal vein, respectively. At 0.083, 0.25, 0.5, 1, 2, 4 and 8 h after injection, blood samples of 4 animals in each group were collected, and tissues, including brain, heart, liver, spleen, lungs and kidneys, were collected, washed and weighed. The amount of coumarin-6 in those samples was quantified by Benny's method with a little modification (21). Briefly, blood or tissue samples were homogenized in 5-fold (for brain) or 10-fold (for serum and other tissues) volume of RIPA/acetonitrile (1:1, *v/v*) to extract coumarin-6, and centrifuged (15,000 g ×15 min, 4°C) to remove de-natured proteins. The supernatants were carefully collected and detected with NOVOstar microplate reader (Ex/Em = 450/510 nm). The results were normalized to the tissue weights in the corresponding samples.

For qualitative study, ICR mice were dosed with CMs or CS via the caudal vein at 0.4 mg/kg body weight, respectively. The animals were anaesthetized 1 h post-injection and sequentially perfused with 0.9% saline and 4% paraformaldehyde. Then, the brains were collected and fixed in 4% paraformaldehyde overnight. Thereafter, brains were sequentially dehydrated with 15% and 30% sucrose PBS solution for 12 h and 24 h, and brain cryostat sections (20 μm) were prepared. The sections were stained with propidium iodide (PI) (2 μg/ml), washed with PBS, mounted in Dako fluorescent mounting medium and observed with the fluorescence microscope (IX51, Olympus, Japan).

Statistical Analysis

Statistical analysis was performed using Student's *t* test. The differences were considered significantly for $p < 0.05$.

RESULTS

Synthesis and Characterization of PCL-PEEP

An amphiphilic copolymer PCL-PEEP was synthesized by ring-opening polymerization of EEP using PCL_{31}-OH as initiator in this work. The average degree of polymerization (DP) of PEEP was 43 according to ^{1}H-NMR spectrum based on the integration ratio of peaks at 4.16 and 4.26 ppm (6H) to peak at 2.30 ppm (2H), assigned to

methylene groups of PEEP block and PCL block, respectively (Fig. 1A). The *Mn* of PCL-PEEP determined by ^{1}H NMR was 10,180 Da, which was a bit lower than the theoretical value (11,040 Da). The typical GPC chromatogram of PCL-PEEP is shown in Fig. 1B. The *M*n, *M*w and PDI of PCL-PEEP were 33,140 Da, 53,140 Da and 1.60, respectively. Fig. 1C demonstrates the fluorescence-excitation spectrum of pyrene in PCL-PEEP micelles at different concentrations. The red shift of fluorescence due to the incorporation of pyrene into micelles indicated that the CMC of PCL-PEEP was 0.51 μg/ml. The low CMC of PCL-PEEP ensured its *in vivo* application as DDS, because the micelles would not disassemble while diluted by plasma after the intravenous injection.

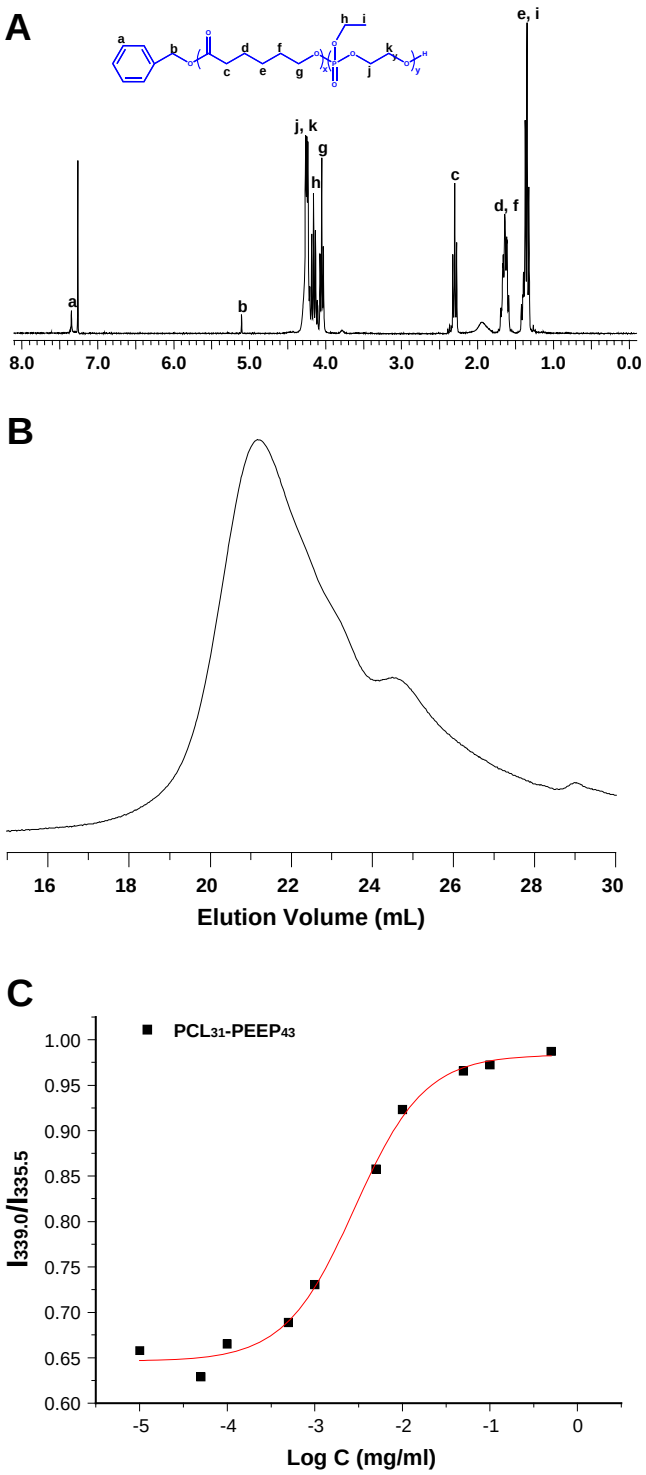

Fig. 1 ^{1}H NMR spectrum (**A**), Gel Permeation Chromatogram (**B**) of PCL-PEEP and intensity ratio ($I_{339.0}/I_{335.5}$) as a function of concentration of PCL-PEEP (**C**).

Preparation and Characterization of CMs

CMs prepared by dialysis method were small and round (Fig. 2). The volume-weighted mean diameter of CMs was 19.4±4.2 nm (n=5), and the size distribution was relatively narrow with typical variance = 0.104 (Fig. 2A). The AFM image revealed that CM was flattened round species, thus confirming the spherical shape of micelles in solution (Fig. 2B). The diameter of typical CMs observed by AFM was around 20 nm, which was in good agreement with the volume-weighted mean diameter determined by dynamic light scattering method. The ζ potential of CMs was −2.41±1.03 mV in deioned water (n=5).

The final concentrations of coumarin-6 and PCL-PEEP in CMs solution after filtration were about 50 μg/ml and 10 mg/ml, respectively. The EE and DLC of CMs were 92.5±0.7% and 0.501±0.004%, respectively, and CMs were relatively stable during 24 h incubation in both HBSS and DMEM with 10% FBS. No precipitation was observed during the whole incubation, and the leakage of incorporated coumarin-6 in DMEM with 10% FBS was much faster than that in HBSS (Fig. 2C). However, only 6% and 25% of incorporated coumarin-6 was released to DMEM with 10% FBS at 1 h and 24 h, respectively. The high encapsulation efficiency and low coumarin-6 leakage could be due to the hydrophobic interaction between coumarin-6 and the PCL block. Therefore, PCL-PEEP was an ideal carrier for hydrophobic drugs resulting from its easy preparation, narrow size distribution and high encapsulation efficiency.

Establishment and Characterization of *In Vitro* BBB Model

The typical phenotype of confluent rat BMECs was observed after 6–7 days cultivation as shown in Fig. 3A. Von Willebrand factor, an endothelial cell maker, was expressed by all cells (Fig. 3B), which indicated that the cells were highly purified. The expression of tight junction-associated proteins occludin (Fig. 3C) demonstrated the formation of marginal membrane localization. Alexa Fluor 532-phalloidin staining (Fig. 3D) presented the actin cytoskeleton underlying the cell membrane and forming a

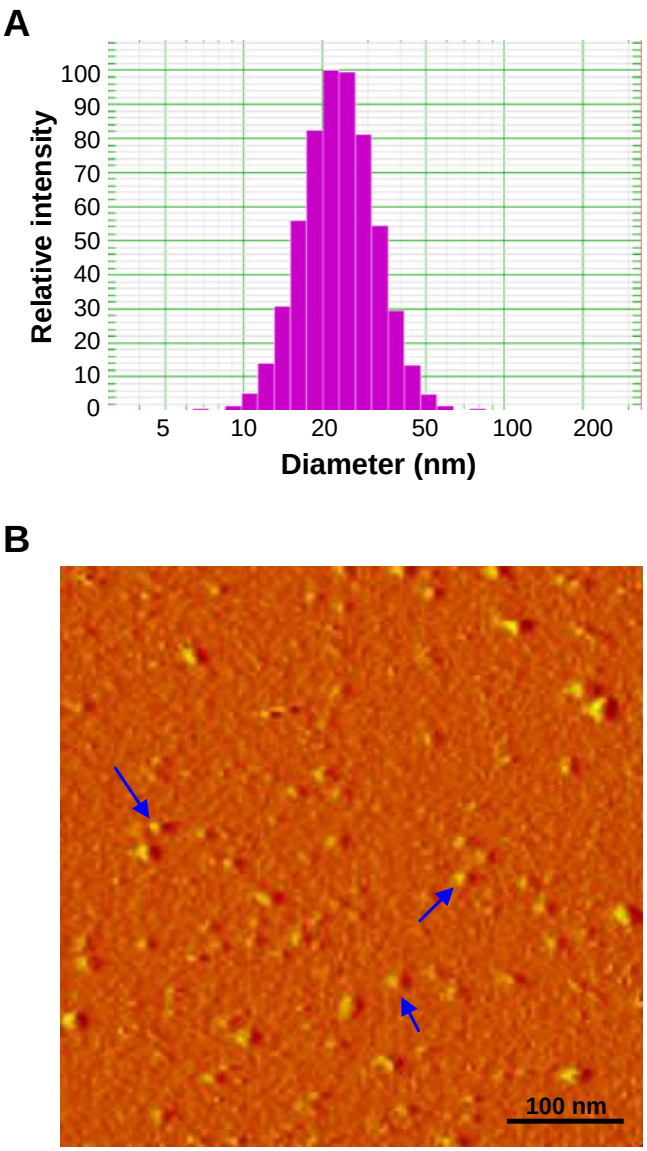

◀**Fig. 2** Typical size distribution (**A**) and morphology (**B**) of CMs determined by dynamic light scattering and atomic force microscope, and in vitro release of coumrain-6 from CMs in HBSS and DMEM containing 10% FBS (**C**). Arrows, CMs.

prominent continuous band at the cell borders. The high expression of P-glycoprotein was evidenced by the survival of BMECs at the presence of 3 μg/ml puromycin in culture. The TEER of BMECs layer could reach higher than 300 Ωcm^2, which suggested low paracellular transport. These results indicated that the *in vitro* model of BBB was successfully established.

Cellular Uptake of CMs by BMECs

The time-, temperature- and concentration-dependent uptake of CMs was investigated on BMECs. As shown in Fig. 4A, the uptake of CMs and CS were both time-dependent, but more efficient endocytosis was observed on CMs, which was 1.4-fold of CS after 4 h incubation. The endocytosis of CMs was greatly inhibited under 4°C, while the uptake of CS was not significantly affected, suggesting that the uptake of CMs, but not CS, was temperature-dependent. The concentration-dependent endocytotic profiles of CMs and CS were rather different as shown in Fig. 4B. The endocytosis of CMs was effective at low concentration (5 and 50 ng/ml), and a plateau was reached above 200 ng/ml. On the contrary, when the feeding CS concentration increased, the endocytosis of CS increased significantly even at high dose. The result could be explained by the difference in endocytosis mechanism that CMs were actively uptaken, while CS was passively diffused into BMECs.

Cytotoxicity of BMs to BMECs

MTT method was employed to evaluate the cytotoxicity of BMs (around 20 nm) upon BMECs. As shown in Fig. 5A, no discernable toxicity was observed even at 2 mg/ml, which was far beyond the practical dosage. Furthermore, the TEER of BBB model did not decrease significantly after 24 h incubation, which demonstrated the integrity of the model and therefore the safety of BMs (Fig. 5B). The results demonstrated the low toxicity of BMs to BBB, which, together with its biodegradability and non-toxic degradation products, favors the further application of micelles as drug delivery system.

Brain Distribution of CMs

The biodistribution of CMs in brain was qualitatively investigated using fluorescence microscope, and the presence of coumarin-6 in brain was evidenced by green spots. As shown in Fig. 6, the fluorescence of coronal

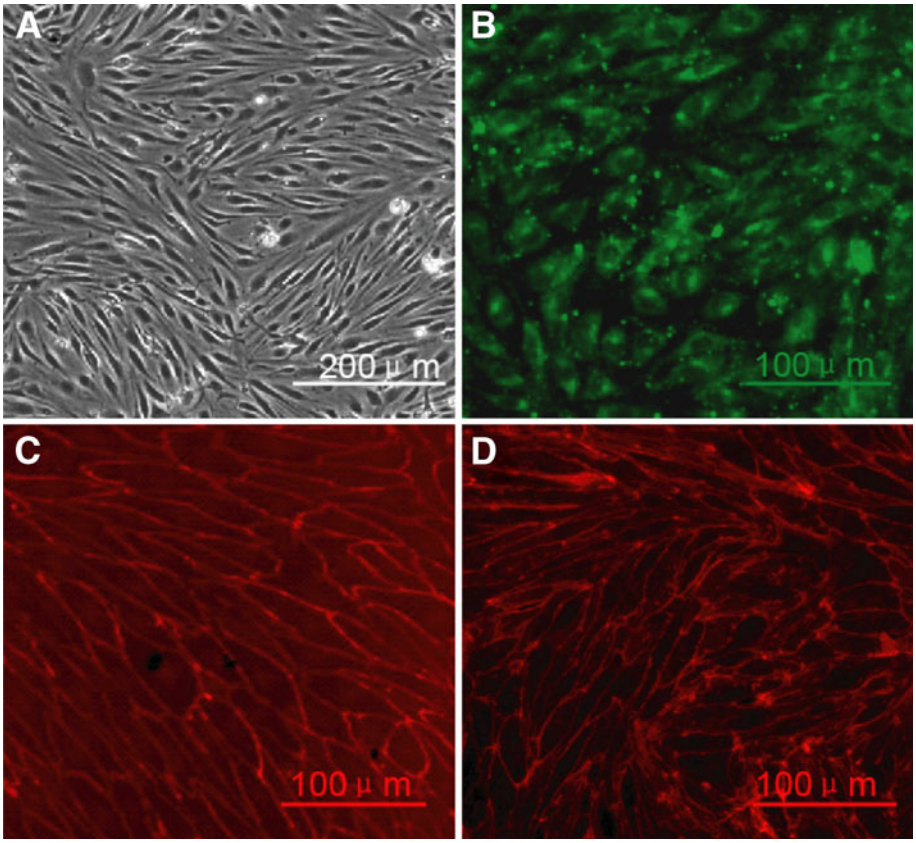

Fig. 3 Characterization of primary rat BMECs (8-day-old) by phase contrast image (**A**) and immunofluorescent staining with anti-von Willebrand factor (**B**), anti-occludin (**C**) and anti-F-actin (**D**) antibodies.

sections from CM-treated mice was more intense than that of CS-treated mice, especially in hippocampus and striatum. The result could be explained by the difference of blood vessel size in different brain regions. It was reported that average blood vessel size in hippocampus and striatum was larger; thus, these regions are more accessible than others (25).

The concentration of coumarin-6 in serum and tissues in CM- or CS-treated mice was quantitatively determined with a NOVOstar microplate reader by recording the fluorescence intensity at 510 nm. The time-dependent variation of coumarin-6 in serum and tissues is shown in Fig. 7, and the maximum concentration (C_{max}), time to maximum concentration (t_{max}), and area under the curve (AUC) are summarized in Table 1. The AUC of CMs was nearly 60% larger than that of CS in brain, whereas the AUC of CMs in liver, lung and spleen was much lower. In accordance with qualitative study, CMs significantly enhanced the accumulation of coumarin-6 in brain. The C_{max} of CMs in brain was 4.74% of injected dose/g tissue (ID/g), which was 2.6-fold of CS. Meanwhile, PCL-PEEP micelles decreased the clearance of coumarin-6 by liver, lungs and spleen, which were usually referred to as reticulo-endothelial system (RES). Thus, micelles composed of PCL-PEEP could be a promising carrier for brain drug delivery.

DISCUSSION

In the last few decades, despite advances in drug discovery and development, there has been little improvement in the treatment of patients with CNS disorders, which could at least partially result from the inability to deliver therapeutic agents across BBB and to reach the target site further. Nanotechnology in pharmacology allows real progress to achieve spatial site-specific delivery (26). Nanocarriers can enhance drug delivery through 1) increasing the local drug gradient at BBB by passive targeting, 2) allowing drug-trafficking by non-specific or receptor-mediated endocytosis, and 3) blocking drug efflux transporters at the BBB (27). PEEP showed good affinity with neuron and osteoblast during its application in tissue engineering, which the authors believed was due to its hydrophilicity and its effect on promoting cell attachment (15, 28). The affinity of PEEP for biomolecules could be attributed to increased local drug gradient at BBB and facilitate non-specific endocytosis. For the reasons above, in the present work, micelles composed of biodegradable amphiphilic block copolymer PCL-PEEP were first evaluated as potential DDS targeting to the brain.

PCL-PEEP can self-assemble into about 20 nm spherical particles and encapsulate hydrophobic drugs into the inner core composed of PCL. The CMC value of PCL-PEEP was

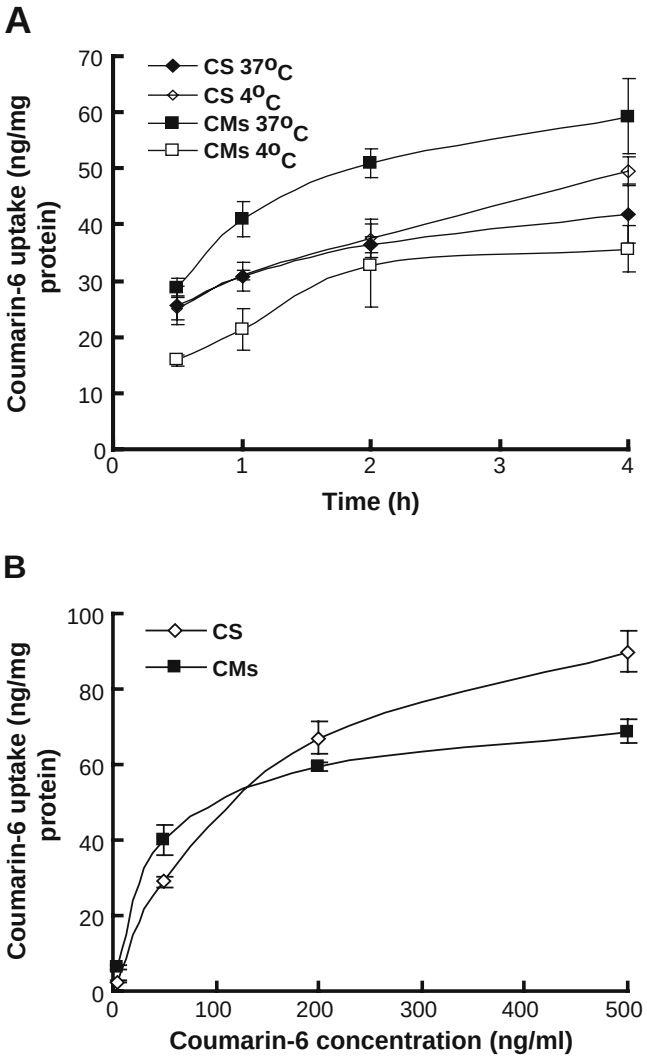

Fig. 4 Time-, temperature- (**A**) and concentration- (**B**) dependent uptake of CS or CMs by BMECs. Data represented the mean ± S.D. ($n=3$).

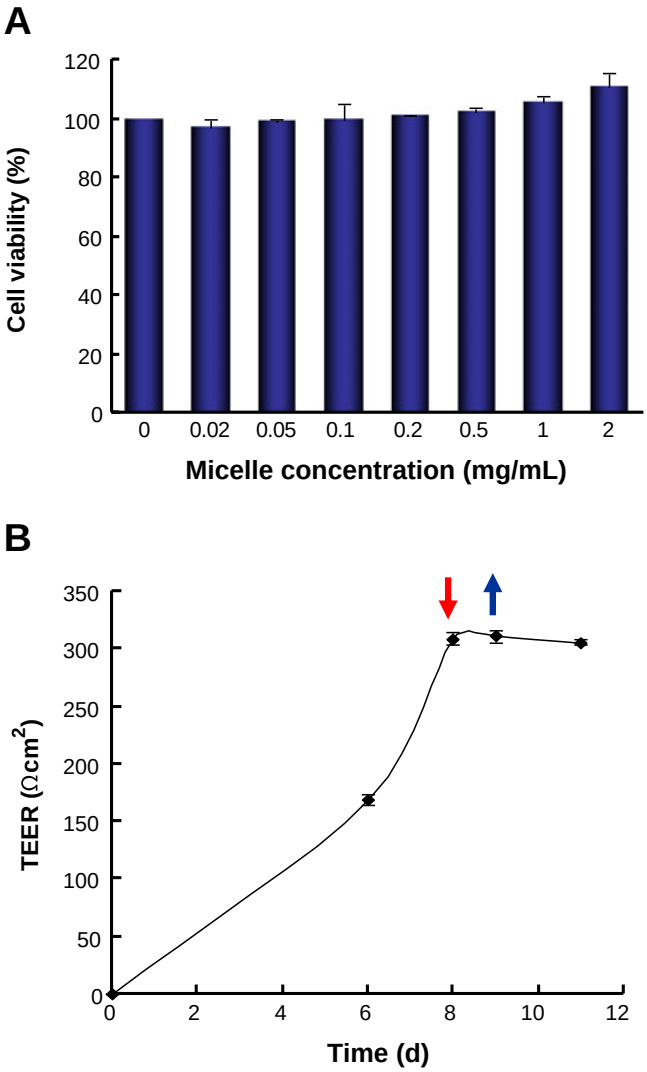

Fig. 5 The *in vitro* cytotoxicity of BMs on BMECs at concentration ranging from 0.02 to 2 mg/ml (**A**) and on BBB model at 2 mg/ml (**B**). The *red* and *blue arrows* indicated the addition and removal of micelles, respectively. Data represented the mean ± S.D. ($n=3$).

0.51 μg/ml. The leakage of courmarin-6 was only 6% and 25% after 1 h and 24 h incubation in DMEM (containing 10% FBS), which was in accordance with the release profile of coumarin-6-loaded nanoparticles reported by Hu *et al.* (4). Higher leakage of CMs in 10% FBS containing DMEM than HBSS could result from the solubilization of coumarin-6 by FBS (29). Because the CMs were freshly prepared before use, it was positive that most of coumarin-6 was still entrapped in CMs during the *in vitro* and *in vivo* evaluation process.

A functional BBB model is helpful for the evaluation of DDS aiming to deliver drug to CNS. Immortalized rat brain capillary endothelial cell lines (such as RBE4, CR3 and bEnd.3) have usually been used for BBB establishment. Unfortunately, none of these cell lines generated the necessary restrictive paracellular barrier properties (30), and did not closely represent the *in vivo* situation. As a result, primary brain microvessel endothelial cells (BMECs) were favored. However, the establishment of BBB model requires highly pure primary BMECs, but the yield of primary BMECs from the species of rat with general isolation methods was so low that it was insufficient for high throughput permeability experiments (30). In our study, the yield and purity of BMECs were efficiently improved through several strategies based on the difference between cells in attachment time and P-gp expression level (24, 31, 32). Mainly, the rinse procedure after 4 h incubation could remove the contaminant cells and single endothelial cells which cannot proliferate to form confluent monolayer but

Fig. 6 Serum and tissue concentration–time profiles of coumarin-6 following i.v. injection of CS or CMs at a dose of 0.40 mg/kg in mice (**A**-**G**) and the comparison of coumarin-6 distribution in tissues 1 h post injection (**H**). Data represented the mean ± S.D. $n=4$. ** $p<0.001$.

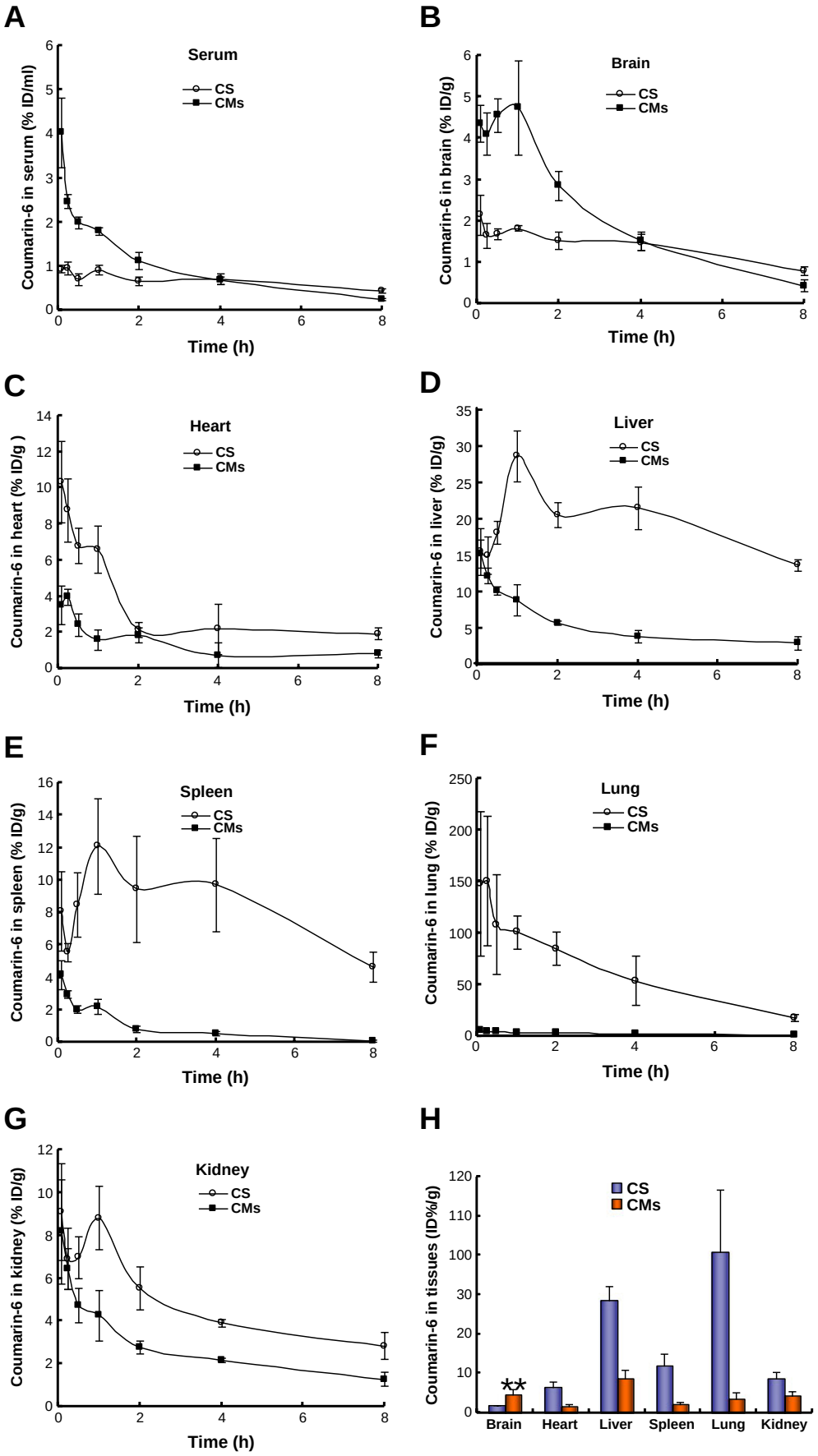
A
Serum
CS
CMs
Coumarin-6 in serum (% ID/ml)
Time (h)
B
Brain
CS
CMs
Coumarin-6 in brain (% ID/g)
Time (h)
C
Heart
CS
CMs
Coumarin-6 in heart (% ID/g)
Time (h)
D
Liver
CS
CMs
Coumarin-6 in liver (% ID/g)
Time (h)
E
Spleen
CS
CMs
Coumarin-6 in spleen (% ID/g)
Time (h)
F
Lung
CS
CMs
Coumarin-6 in lung (% ID/g)
Time (h)
G
Kidney
CS
CMs
Coumarin-6 in kidney (% ID/g)
Time (h)
H
CS
CMs
Coumarin-6 in tissues (ID%/g)
**
Brain
Heart
Liver
Spleen
Lung
Kidney

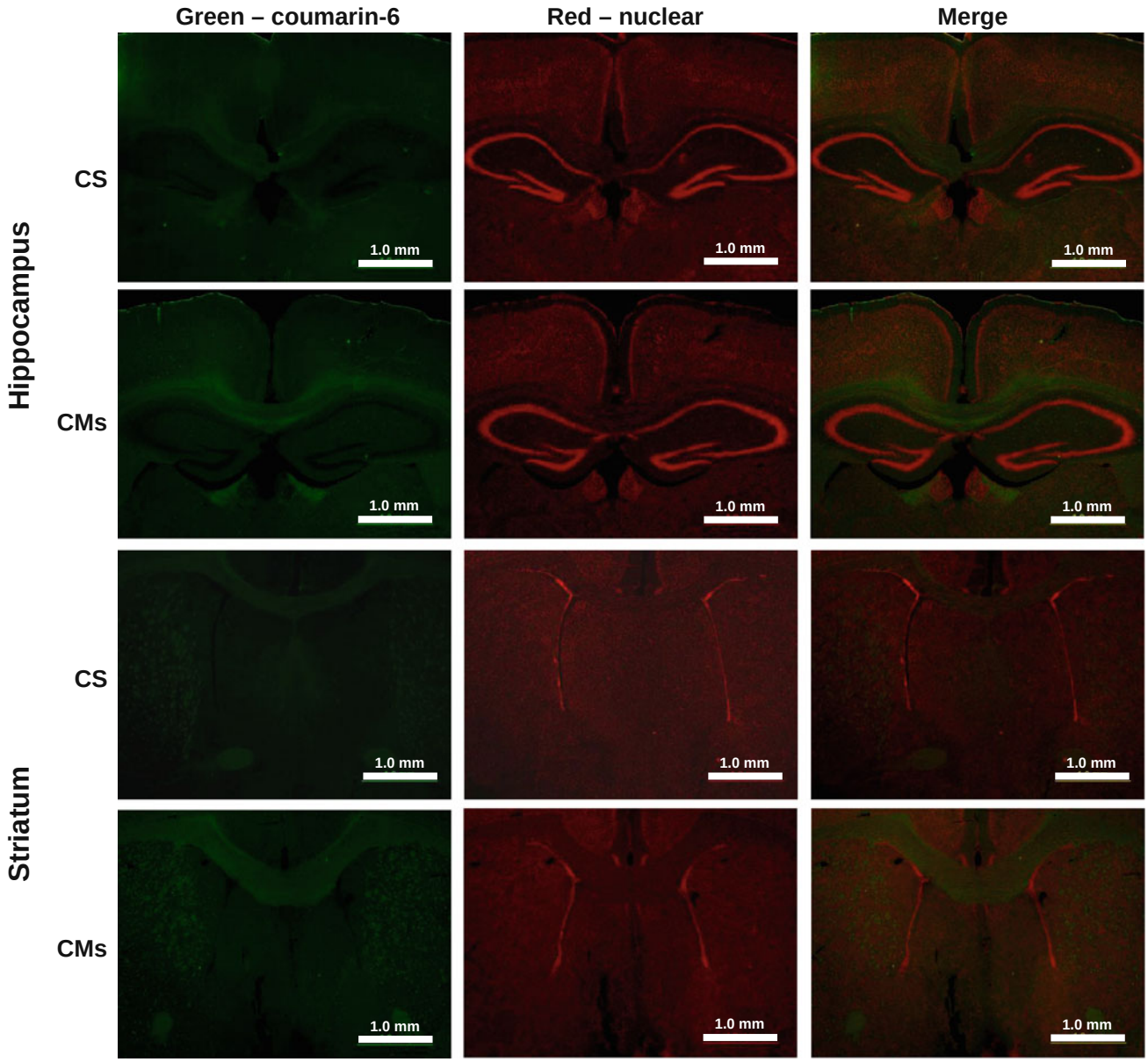

Fig. 7 The qualitative evaluation of coumarin-6 in brain region of hippocampus and striatum 1 h post intravenous injection of CS or CMs at a dose of 0.40 mg/kg coumarin-6. *Green*: coumarin-6. *Red*: PI stained nuclei. The magnification bar is 1 mm.

Table 1 Pharmacokinetic Parameters of Coumarin-6 in Serum and Tissues After Intravenous Injection of CS or CMs in Mice. Data Represented the Mean ± S.D. $n = 4$

PK parameters	T_{max} (h)		C_{max} (%ID/g or %ID/ml)		$AUC_{(0\text{-}t)}$ (%ID/g·h or %ID/ml·h)	
	CS	CMs	CS	CMs	CS	CMs
Brain	0.083	1	2.14 ± 0.48	4.74 ± 1.14**	10.79	16.13
Serum	0	0	–	–	5.20	7.11
Heart	0.083	0.25	10.31 ± 2.27	3.95 ± 0.44*	23.73	9.75
Liver	1	0.083	28.67 ± 3.47	15.22 ± 1.96**	155.47	40.45
Spleen	1	0.083	12.09 ± 2.95	4.14 ± 0.87*	66.58	6.25
Lung	0.25	0.083	150.44 ± 63.11	5.26 ± 1.13*	411.73	19.23
Kidney	0.083	0.083	9.10 ± 2.27	8.16 ± 2.42	37.06	20.15

*$p < 0.01$ compared with CS, **$p < 0.001$ compared with CS

not the fully attached microvessels. Puromycin, a supplement in culture medium, is a P-gp substrate and is cytotoxic to the cells lacking P-gp if puromycin is metabolized in the cells into puromycin aminonucleoside. BMECs, but not the contaminating cells, express high level of P-gp; thus, only BMECs can survive at the presence of puromycin. The barrier properties of BMECs were induced by adding hydrocortisone, hEGF, VEGF, hFGF-B, R3-IGF-1 and ascorbic acid, which modulated the paracellular permeability of BMECs (33–38). The expression of marker proteins, such as Von Willebrand antigen, occluding and F-actin (Fig. 3) by BMECs and higher TEER of BMECs monolayer than frequently reported values (around 160–200 Ωcm^2) (39–41), demonstrated the successful establishment of BBB model.

The cytotoxicity of BMs on BMECs was evaluated. The effect of BMs on permeability of BBB was also investigated because the increasing permeability of BBB leads to adverse effects, such as seizures and chronic neuropathological changes (42). Our results demonstrated that BMs did not affect the cell viability of BMEC. It is noteworthy that the permeability of BBB was not increased, even exposed to BMs at 2 mg/ml. These results proved good *in vitro* safety of BMs and ensured its further application in CNS-targeting drug delivery.

Taking advantage of the efficient model establishment, the cellular uptake of CS and CMs was evaluated on this model. Our results indicated that the uptake of CMs was temperature dependent, which was in accordance with that reported by Hu *et al.* (4). It is generally accepted that temperature dependence indicates an active uptake process (43), thus CM was actively endocytosed by BMECs but not CS. A recent study on nanoparticle uptake in living endothelial cells by Wang *et al.* indicated that bovine serum albumin (BSA)-coated small particles (20 nm) were more prone to be endocytosed through caveolae-dependent pathway than large ones (40 nm and 100 nm) (44). As PEEP showed affinity to biomolecules as we discussed above, CMs could be coated with serum proteins and therefore endocytosed by BMECs through caveolae-dependent pathway. However, the precise endocytosis mechanism of PCL-PEEP micelles needs further investigation. The uptake of CMs by BMECs increased rapidly with concentration of CMs increasing from 5 to 50 ng/ml. However, when the concentration of CMs increased to 500 ng/ml, a flattening of the curve occurred. The saturation could result from the depletion of endocytotic mechanism as observed by Lorenz *et al.* in their study on uptake of polyisoprene nanoparticles (45). Although the passive diffusion of coumarin-6 released from CMs could coexist, it only took up a small portion because of relatively short incubation time. Furthermore, free coumarin-6 in incubation media was not uptaken as efficiently as CMs.

The biodistribution of coumarin-6 in brain was determined qualitatively and quantitatively, both of which indicated that high brain accumulation of CMs was achieved. The maximum concentration (C_{max}) in brain was 364.4 ng/g (4.75% ID/g), which was much higher than most previously reported nanoparticles (4–9). Because brain capillary blood volume and endothelial cell volume represent only approximately 1% and 0.1% of the total volume of brain according to the literature (46), the speculation that the high brain distribution was due to the CMs in brain capillary blood and BMECs was not correct. As CMs lack purposely designed ligands that facilitate transcytosis across BBB, the difference in physico-chemical characteristics between these carriers may be the most possible explanation (24). Recently, Sonavane *et al.* found that the brain accumulation of 15 nm gold nanoparticles was higher than three other gold nanoparticles (50 nm, 100 nm and 200 nm) (10). A similar phenomenon was also observed by Gao *et al.*, who were investigating the influence of particle size on transport of methotrexate-loaded polybutylcyanoacrylate nanoparticles across blood brain barrier (11). CMs were about 20 nm, which was much smaller than those reported nanoparticles (>100 nm) (4–9). Recently, De Jong *et al.* reported the effect of particle size on biodistribution (47). According to their result, the smallest 10 nm particles showed the most widespread biodistribution, and were also the only particles showing brain distribution. Thus, the particle size could be the most important characteristic that affects the biodistribution of nanocarriers. Another possible reason for high brain distribution of CMs was the absorption of serum protein. Apoliprotein, by coating on Tween-80-decorated nanoparticles, was proved to enhance nanoparticle brain accumulation by Kreuter *et al.* (6, 9, 48–50). As PEEP showed good affinity with biomolecules as discussed above (15, 28), it is reasonable to presume that the interaction between PEEP and apoliprotein was possible. Furthermore, the affinity of CMs with biomolecules could also be attributed to CM retention in brain blood vessels, which consequently increases the local concentration of CMs. Thus, we presumed the particle size and hydrophilic outer layer composed of PEEP played an important role in enhanced brain distribution, although the precise mechanism needs further investigation.

CONCLUSION

PCL-PEEP could self-assemble into 20 nm spherical particles with high encapsulation efficiency of coumarin-6 and good stability. The uptake of CMs by BMECs was efficient, especially at low concentration. The micelles did not affect the cell viability and barrier property of the model. CMs showed high brain distribution with 4.74%ID/g

brain, which was 2.6-fold of CS. In addition, the CMs are prone to accumulate in hippocampus and striatum. These results suggested that PCL-PEEP micelles were a promising biocompatible brain drug delivery system with low toxicity.

ACKNOWLEDGEMENTS

The National Basic Research Program of China (2007CB935804 and 2009CB930304), National Natural Science Foundation of China (90713035), and National Science & Technology Major Project "Key New Drug Creation and Manufacturing Program"(No 2009ZX09501-024 and 2009ZX09103-066), and Major project of Shanghai Science and Technology Committee (08DZ1980200) are gratefully acknowledged for financial support.

REFERENCES

1. Pardridge WM. Brain drug development and brain drug targeting. Pharm Res. 2007;24:1729–32.
2. Garcia-Garcia E, Andrieux K, Gil S, Couvreur P. Colloidal carriers and blood-brain barrier (BBB) translocation: a way to deliver drugs to the brain? Int J Pharm. 2005;298:274–92.
3. Jones AR, Shusta EV. Blood-brain barrier transport of therapeutics via receptor-mediation. Pharm Res. 2007;24:1759–71.
4. Hu K, Li JW, Shen YH, Lu W, Gao XL, Zhang QZ, *et al.* Lactoferrin-conjugated PEG-PLA nanoparticles with improved brain delivery: *in vitro* and *in vivo* evaluations. J Control Release. 2009;134:55–61.
5. Huwyler J, Wu DF, Pardridge WM. Brain drug delivery of small molecules using immunoliposomes. Proc Natl Acad Sci USA. 1996;93:14164–9.
6. Gulyaev AE, Gelperina SE, Skidan IN, Antropov AS, Kivman GY, Kreuter J. Significant transport of doxorubicin into the brain with polysorbate 80-coated nanoparticles. Pharm Res. 1999;16:1564–9.
7. Ambruosi A, Yamamoto H, Kreuter J. Body distribution of polysorbate-80 and doxorubicin-loaded [14C]poly(butyl cyanoacrylate) nanoparticles after i.v. administration in rats. J Drug Target. 2005;13:535–42.
8. Pang ZQ, Lu W, Gao HL, Hu KL, Chen J, Zhang CL, *et al.* Preparation and brain delivery property of biodegradable polymersomes conjugated with OX26. J Control Release. 2008;128:120–7.
9. Ambruosi A, Khalansky AS, Yamamoto H, Gelperina SE, Begley DJ, Kreuter J. Biodistribution of polysorbate 80-coated doxorubicin-loaded [14C]-poly(butyl cyanoacrylate) nanoparticles after intravenous administration to glioblastoma-bearing rats. J Drug Target. 2006;14:97–105.
10. Sonavane G, Tomoda K, Makino K. Biodistribution of colloidal gold nanoparticles after intravenous administration: effect of particle size. Colloids Surf B Biointerfaces. 2008;66:274–80.
11. Gao KP, Jiang XG. Influence of particle size on transport of methotrexate across blood brain barrier by polysorbate 80-coated polybutylcyanoacrylate nanoparticles. Int J Pharm. 2006;310:213–9.
12. Otsuka H, Nagasaki Y, Kataoka K. PEGylated nanoparticles for biological and pharmaceutical applications. Adv Drug Deliv Rev. 2003;55:403–19.
13. Liu LH, Guo K, Lu J, Venkatraman SS, Luo D, Ng KC, *et al.* Biologically active core/shell nanoparticles self-assembled from cholesterol-terminated PEG-TAT for drug delivery across the blood-brain barrier. Biomaterials. 2008;29:1509–17.
14. Kuroda JI, Kuratsu JI, Yasunaga M, Koga Y, Saito Y, Matsumura Y. Potent antitumor effect of SN-38-incorporating polymeric micelle, NK012, against malignant glioma. Int J Cancer. 2009;124:2505–11.
15. Fruijtier-Polloth C. Safety assessment on polyethylene glycols (PEGs) and their derivatives as used in cosmetic products. Toxicology. 2005;214:1–38.
16. Chaubal MV, Sen Gupta A, Lopina ST, Bruley DF. Polyphosphates and other phosphorus-containing polymers for drug delivery applications. Crit Rev Ther Drug Carrier Syst. 2003;20:295–315.
17. Wang S, Wan ACA, Xu XY, Gao SJ, Mao HQ, Leong KW, *et al.* A new nerve guide conduit material composed of a biodegradable poly(phosphoester). Biomaterials. 2001;22:1157–69.
18. Zhao Z, Wang J, Mao HQ, Leong KW. Polyphosphoesters in drug and gene delivery. Adv Drug Deliv Rev. 2003;55:483–99.
19. Wang YC, Liu XQ, Sun TM, Xiong MH, Wang J. Functionalized micelles from block copolymer of polyphosphoester and poly (epsilon-caprolactone) for receptor-mediated drug delivery. J Control Release. 2008;128:32–40.
20. Wang YC, Tang LY, Sun TM, Li CH, Xiong MH, Wang J. Self-assembled micelles of biodegradable triblock copolymers based on poly(ethyl ethylene phosphate) and poly(-caprolactone) as drug carriers. Biomacromolecules. 2008;9:388–95.
21. Benny O, Fainaru O, Adini A, Cassiola F, Bazinet L, Adini I, *et al.* An orally delivered small-molecule formulation with antiangiogenic and anticancer activity. Nat Biotechnol. 2008;26:799–807.
22. Song WJ, Du JZ, Liu NJ, Dou S, Cheng J, Wang J. Functionalized diblock copolymer of poly(epsilon-caprolactone) and polyphosphoester bearing hydroxyl pendant groups: synthesis, characterization, and self-assembly. Macromolecules. 2008;41:6935–41.
23. Demeuse P, Kerkhofs A, Struys-Ponsar C, Knoops B, Remacle C, de Aguilar PV. Compartmentalized coculture of rat brain endothelial cells and astrocytes: a syngenic model to study the blood-brain barrier. J Neurosci Methods. 2002;121:21–31.
24. Calabria AR, Weidenfeller C, Jones AR, de Vries HE, Shusta EV. Puromycin-purified rat brain microvascular endothelial cell cultures exhibit improved barrier properties in response to glucocorticoid induction. J Neurochem. 2006;97:922–33.
25. Patt S, Sampaolo S, TheallierJanko A, Tschairkin I, CervosNavarro J. Angiogenesis triggered by severe chronic hypoxia displays regional differences. J Cereb Blood Flow Metab. 1997;17:801–6.
26. Mikhail AS, Allen C. Block copolymer micelles for delivery of cancer therapy: transport at the whole body, tissue and cellular levels. J Control Release. 2009;138:214–23.
27. Wong HL, Chattopadhyay N, Wu XY, Bendayan R. Nanotechnology applications for improved delivery of antiretroviral drugs to the brain. Adv Drug Deliv Rev. 2010;62:503–17.
28. Yang XZ, Sun TM, Dou S, Wu J, Wang YC, Wang J. Block copolymer of polyphosphoester and poly(L-lactic acid) modified surface for enhancing osteoblast adhesion, proliferation, and function. Biomacromolecules. 2009;10:2213–20.
29. Kratochwil NA, Huber W, Muller F, Kansy M, Gerber PR. Predicting plasma protein binding of drugs: a new approach. Biochem Pharmacol. 2002;64:1355–74.
30. Gumbleton M, Audus KL. Progress and limitations in the use of *in vitro* cell cultures to serve as a permeability screen for the blood-brain barrier. J Pharm Sci. 2001;90:1681–98.
31. Bowman PD, Ennis SR, Rarey KE, Betz AL, Goldstein GW. Brain microvessel endothelial cells in tissue culture: a model for study of blood-brain barrier permeability. Ann Neurol. 1983;14:396–402.
32. Perriere N, Demeuse PH, Garcia E, Regina A, Debray M, Andreux JP, *et al.* Puromycin-based purification of rat brain capillary

endothelial cell cultures. Effect on the expression of blood-brain barrier-specific properties. J Neurochem. 2005;93:279–89.
33. Borges N, Shi F, Azevedo I, Audus KL. Changes in brain microvessel endothelial cell monolayer permeability induced by adrenergic drugs. Eur J Pharmacol. 1994;269:243–8.
34. Flores-Benitez D, Ruiz-Cabrera A, Flores-Maldonado C, Shoshani L, Cereijido M, Contreras RG. Control of tight junctional sealing: role of epidermal growth factor. Am J Physiol Renal Physiol. 2007;292:F828–36.
35. Wang W, Dentler WL, Borchardt RT. VEGF increases BMEC monolayer permeability by affecting occludin expression and tight junction assembly. Am J Physiol Heart Circ Physiol. 2001;280: H434–40.
36. Sobue K, Yamamoto N, Yoneda K, Hodgson ME, Yamashiro K, Tsuruoka N, *et al.* Induction of blood-brain barrier properties in immortalized bovine brain endothelial cells by astrocytic factors. Neurosci Res. 1999;35:155–64.
37. Lopez-Lopez C, LeRoith D, Torres-Aleman I. Insulin-like growth factor I is required for vessel remodeling in the adult brain. Proc Natl Acad Sci USA. 2004;101:9833–8.
38. Lin JL, Huang YH, Shen YC, Huang HC, Liu PH. Ascorbic acid prevents blood-brain barrier disruption and sensory deficit caused by sustained compression of primary somatosensory cortex. J Cereb Blood Flow Metab. 2010;30:1121–36.
39. Raub TJ, Kuentzel SL, Sawada GA. Permeability of bovine brain microvessel endothelial cells *in vitro*: barrier tightening by a factor released from astroglioma cells. Exp Cell Res. 1992;199:330–40.
40. Honda M, Nakagawa S, Hayashi K, Kitagawa N, Tsutsumi K, Nagata I, *et al.* Adrenomedullin improves the blood-brain barrier function through the expression of claudin-5. Cell Mol Neurobiol. 2006;26:109–18.
41. Abbruscato TJ, Davis TP. Combination of hypoxia/aglycemia compromises *in vitro* blood-brain barrier integrity. J Pharmacol Exp Ther. 1999;289:668–75.
42. Zlokovic BV. The blood-brain barrier in health and chronic neurodegenerative disorders. Neuron. 2008;57:178–201.
43. Ragnarsson EGE, Schoultz I, Gullberg E, Carlsson AH, Tafazoli F, Lerm M, *et al.* Yersinia pseudotuberculosis induces transcytosis of nanoparticles across human intestinal villus epithelium via invasin-dependent macropinocytosis. Lab Invest. 2008;88:1215–26.
44. Wang ZJ, Tiruppathi C, Minshall RD, Malik AB. Size and dynamics of caveolae studied using nanoparticles in living endothelial cells. ACS Nano. 2009;3:4110–6.
45. Lorenz MR, Kohnle MV, Dass M, Walther P, Hocherl A, Ziener U, *et al.* Synthesis of fluorescent polyisoprene nanoparticles and their uptake into various cells. Macromol Biosci. 2008;8:711–27.
46. Pardridge WM. Peptide drug delivery to the brain. New York: Raven; 1991. p. 52–3.
47. De Jong WH, Hagens WI, Krystek P, Burger MC, Sips AJAM, Geertsma RE. Particle size-dependent organ distribution of gold nanoparticles after intravenous administration. Biomaterials. 2008;29:1912–9.
48. Alyautdin RN, Petrov VE, Langer K, Berthold A, Kharkevich DA, Kreuter J. Delivery of loperamide across the blood-brain barrier with polysorbate 80-coated polybutylcyanoacrylate nanoparticles. Pharm Res. 1997;14:325–8.
49. Kreuter J, Shamenkov D, Petrov V, Ramge P, Cychutek K, Koch-Brandt C, *et al.* Apolipoprotein-mediated transport of nanoparticle-bound drugs across the blood-brain barrier. J Drug Target. 2002;10:317–25.
50. Steiniger SCJ, Kreuter J, Khalansky AS, Skidan IN, Bobruskin AI, Smirnova ZS, *et al.* Chemotherapy of glioblastoma in rats using doxorubicin-loaded nanoparticles. Int J Cancer. 2004;109:759–67.